The microscopical theory of homogeneous nucleation in alloys: II. Calculations of nucleation parameters for various alloy models

1998 J. Phys.: Condens. Matter 10 2275

(http://iopscience.iop.org/0953-8984/10/10/010)

J. Phys.: Condens. Matter **10** (1998) 2275–2290. Printed in the UK PII: S0953-8984(98)88195-2

The microscopical theory of homogeneous nucleation in alloys: II. Calculations of nucleation parameters for various alloy models

V Yu Dobretsov†§ and V G Vaks‡

† Centre d'Etudes de Saclay, Section de Recherches de Métallurgie Physique, 91191 Gif-sur-Yvette Cédex, France

‡ Russian Research Centre 'Kurchatov Institute', Moscow 123182, Russia

Received 6 October 1997

Abstract. The earlier-described microscopical theory of homogeneous nucleation in alloys is used to calculate the nucleation rate and the critical embryo parameters for several alloy models. The results of the calculations provide both qualitative and quantitative information about the characteristics of nucleation in alloys and their variations with the supersaturation s, the temperature T, and the inter-atomic interaction range r_{int}. Several approximations of various levels of sophistication are used to treat the composition fluctuation effects which are shown to be usually important for the thermodynamics of nucleation. With increasing supersaturation or temperature the nucleation barrier lowers and the embryo interface with the exterior phase gets more diffuse, in agreement with the results of previous treatments, but making allowance for the fluctuative effects provides significant quantitative refinements for the results. The limitations of the conventional theories of nucleation due to neglecting the interaction of different embryos are discussed, and their region of validity, depending on the parameters s, T, and r_{int}, is estimated.

1. Introduction

In the preceding paper [1] (to be referred to as I) we discussed the theory of the homogeneous nucleation in metastable states of alloys. When the number of embryos of the new phase in the metastable state is small and their interaction with each other is negligible, the nucleation rate J, i.e. the number of critical and supercritical embryos being formed in unit volume per unit time, is usually described by the Zeldovich–Volmer equation derived by Zeldovich in his phenomenological theory [2]:

$$J = J_0 \exp(-\beta\,\Delta\Omega_c). \tag{1}$$

Here $\beta = 1/T$ is the reciprocal temperature, $\Delta\Omega_c$ is the activation barrier for the formation of the critical embryo, and the prefactor J_0 is determined by the kinetic characteristics. In most theoretical treatments of nucleation, the quantities $\Delta\Omega_c$ and J_0 are considered as phenomenological parameters. Microscopical estimates of the nucleation barrier $\Delta\Omega_c$ based on a simplified approach have been made by Cahn and Hilliard [3]. As was discussed in I, these estimates yielded important qualitative information—in particular, about the variation of the properties of critical embryos and the $\Delta\Omega_c$ values with the supersaturation of the initial metastable state. However, no discussion of the prefactor J_0 in (1), or of possible

§ Permanent address: Russian Research Centre 'Kurchatov Institute', Moscow 123182, Russia.

0953-8984/98/102275+16$19.50

errors of the approach used and its validity region, and no estimates for solid alloys have been given in reference [3].

At the same time, experimental studies of the homogeneous nucleation encounter difficulties, in particular, as it is usually difficult to separate it from the heterogeneous nucleation at various impurities, interfaces, lattice defects in solids, etc. Therefore, information on the critical embryos and the parameters $\Delta\Omega_c$ and J_0 for real systems—in particular, for alloys—is rather scarce as yet.

In I we developed the microscopical theory of the homogeneous nucleation in alloys in terms of the configurational interactions v_{ij} (used in conventional theories of alloys; see e.g. [5]) and some microscopical kinetic characteristics. In the present work we employ these results to study the properties of the critical embryo, and to calculate the parameters $\Delta\Omega_c$ and J_0 in equation (1) for several simple models of alloys. The results of the calculations provide both qualitative and quantitative information on the scale of the characteristics of nucleation in alloys, as well as on their dependence on external and internal parameters of the system, such as the supersaturation, the temperature, and the inter-atomic interaction range. These results also enable one to estimate the validity region for the conventional approaches to the nucleation theory [1–4], in which the interactions of different embryos are neglected.

In section 2 we describe the main equations and the models used. In section 3 we discuss the methods of our calculations. The results of the calculations are presented in section 4 and are discussed in section 5. The main conclusions are summarized in section 6.

2. The main relations and models used

This work is based on the results and arguments discussed in the previous paper, I. Thus in this section we present only a few basic equations from I which seem to be necessary for understanding the results given below. For all of the details and explanations, we refer the reader to I.

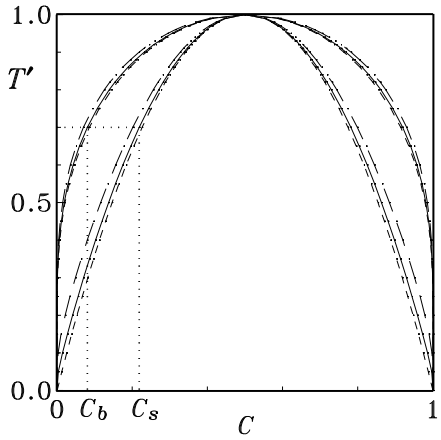

Figure 1. Equilibrium (c, T') phase diagrams, where $T' = T/T_c$ and T_c is the critical temperature. Solid and long-dashed lines show the pair-cluster-approximation (PCA) results for the models fcc-3 and fcc-1, respectively, which are described in section 2; dashed lines show the mean-field-approximation (MFA) results for all of the models. The upper curves are binodals, and the lower curves are spinodals.

We consider the uniform disordered binary alloy A_cB_{1-c} quenched into the metastability region $c_b(T) < c < c_s(T)$ where $c_b(T)$ and $c_s(T)$ are the concentration values at the binodal and the spinodal, respectively (see figure 1). The supersaturation of the metastable state is characterized by its reduced value s, defined as

$$s = \frac{c - c_b(T)}{c_s(T) - c_b(T)}. \tag{2}$$

For variation of c between the binodal and the spinodal, the s-value varies between zero and unity.

The prefactor J_0 in equation (1) is given by equation (I.57):

$$J_0 = \left(\frac{\beta|\gamma_0|}{2\pi}\right)^{1/2} D_{aa}\mathcal{N}D_{\boldsymbol{R}}(\boldsymbol{u}). \tag{3}$$

Here γ_0 is the 'critical', negative eigenvalue in the expression (I.22) for the grand canonical potential $\Omega\{c_i\}$ (where c_i is the mean occupation of the site i by an A-species atom in the non-uniform alloy state under consideration) near its saddle point $c_i = c_i^s$, which corresponds to the critical embryo; D_{aa} given by equation (I.55) is the generalized diffusivity in the 'critical' direction in the c_i-space, which corresponds to the growth of the embryo; $\mathcal{N}$ given by equation (I.43) is the normalizing constant in the embryo size distribution function (I.42); and $D_{\boldsymbol{R}}(\boldsymbol{u})$ is the Jacobian (I.24) of the concentrational variables u_1, u_2, and u_3 in equation (I.20) (which describes the translations of the embryo) with respect to the Cartesian coordinates of its centre, R_1, R_2, and R_3.

The nucleation barrier $\Delta\Omega_c$ is the function $\Delta\Omega\{c_i\}$ given by equation (I.44) at the saddle point values $c_i = c_i^s$:

$$\Delta\Omega_c = F_r\{c_i^s\} - F(c) - \mu(c)\sum_i (c_i^s - c). \tag{4}$$

Here $F_r\{c_i\}$ given by equation (I.45) is the 'reduced' free energy, which does not include the contributions of the fluctuations of the size a and the position $\boldsymbol{R}$ of the embryo; $F(c)$ given by the general expression (I.9) with all c_i equal to c is the free energy of the initial metastable state; and $\mu(c)$ is the chemical potential of this state, which is equal to the derivative $N_s^{-1}\,\partial F(c)/\partial c$ where N_s is the total number of lattice sites.

To get an idea of the scale of the characteristics of the nucleation in alloys, we made calculations based on equations (3) and (4) for several simple models of alloys. The following models have been used.

(i) The nearest-neighbour interaction model for the FCC alloy, to be referred to as the 'fcc-1' model.

(ii) The same model for the BCC alloy, to be referred to as the 'bcc-1' model.

(iii) The FCC alloy model with interactions up to the third neighbour: $v_1 = -1$, $v_2 = -0.8$, and $v_3 = -0.5$, to be referred to as the 'fcc-3' model.

Comparison of the results for the first two models can be used to illustrate the effect of the lattice structure on the nucleation, while a comparison for the fcc-1 and fcc-3 models provides information about the interaction range effect: the mean squared interaction radius $r_{int}^2 = \sum_j v_{ij}r_{ij}^2/\sum_j v_{ij}$ for the model fcc-3 is twice the size of that for the model fcc-1.

3. The methods of calculation

For the free energy $F_r\{c_i\}$ and $F(c)$ in equation (4), we use four different approximations discussed in section 2 of paper I: the ones based on the mean-field approximation (MFA),

F_{MFA} and F_{MFf}, and the ones based on the pair-cluster approximation (PCA), F_{PCA} and F_{PCf}. The chemical potential $\mu(c)$ is determined by equation (I.7) at $c_i = c$ using the chosen approximation for $F(c)$. Employing the MFA in our problem means omitting the fluctuative term F^f in equation (I.45) for both $F_r\{c_i\}$ and $F(c)$. The mean-field-with-fluctuations (MFf) approximation for F_r^f corresponds to using the first-order perturbative expression (I.11) for the fluctuative contribution when the integral over g in (I.36) is taken analytically:

$$F_r^f = \frac{1}{2}\sum_{k\geqslant 4} \ln \frac{\gamma_k}{\gamma_k^0} \tag{5}$$

where γ_k is the same as in equation (I.22), and the γ_k^0 are the eigenvalues of the matrix $\hat{z}$ used in equation (I.40) or (I.47). The MFf fluctuative contribution for the initial uniform state, $F^f(c) = F^f_{\mathrm{MFA}}(c)$, is given by the expression (I.11) for such a case, as mentioned in I. The PCA corresponds to approximating both $F_r\{c_i\}$ and $F(c)$ in equation (4) by the PCA expression (I.12) with $c_i = c_i^s$ and $c_i = c$, respectively. Finally, the pair-cluster-with-fluctuations (PCf) approximation corresponds to employing for $F_r\{c_i\}$ in equation (4) the full equation (I.45) with $F_{ij}(g) = F_{ij}^{\mathrm{PCA}}(g)$ in equation (I.37) given by equation (I.13) at $v_{ij}(g) = g v_{ij}$, and using for $F(c)$ in equation (4) equations (I.16) and (I.13) at $c_i = c$, while the integrations over charge in equations (I.36) and (I.16) are performed numerically.

With the chosen approximation for the free energy $F\{c_i\}$, the calculation starts with finding the structure of the critical embryo, i.e. the saddle point values $c_i = c_i^s$ for the function $\Delta\Omega\{c_i\}$, equation (I.44). The saddle point was found numerically using the standard iterative algorithms with the appropriate choice of the initial distribution c_i^0 for iterations. As it is convenient to use the cubic crystal symmetry $\mathrm{O_h}$ of the system (see below), we considered the $\mathrm{O_h}$-symmetric simulation region within a certain radius R_b, while the values of $c_i = c(\boldsymbol{r}_i)$ for $r_i > R_b$ were assumed to be equal to the initial value c. The R_b-value was taken such that the differences $c_i - c$ at $r_i = R_b$ do not exceed 10^{-3}. This corresponds to R_b-values that are 1.5–2 times the size of the critical embryo radius R_c, and it is sufficient for the results to be virtually independent of R_b.

In calculations using the MFf and PCf approximations, we took into consideration the fact that the fluctuative contribution F^f is treated in these approximations as the first-order perturbative correction [1]. Thus, for consistency of the calculations, the nucleation barrier $\Delta\Omega_c$ in these approximations should be found only within the first order in the fluctuative correction. As the critical embryo corresponds to the saddle point extremum of $\Omega\{c_i\}$, the first-order correction to $\Delta\Omega_c = \Delta\Omega\{c_i^s\}$ corresponds to employing the zero-order values c_{i0}^s for $c_i = c_i^s$ in the rhs of equation (4), i.e. using the MFA values $(c_i^s)_{\mathrm{MFA}}$ in the MFf approximation, and $(c_i^s)_{\mathrm{PCA}}$ in the PCf approximation: taking into account the saddle point shift δc_i^s due to the fluctuative correction results only in a second-order correction in $\Delta\Omega_c$. The prefactor J_0 will be shown to be much less sensitive to the approximations used in the calculations as compared to the exponent in equation (1); thus, in equation (3), the fluctuative corrections were neglected. Therefore, the MFf approximation for $\Delta\Omega_c$ in equation (4) differs from the MFA one only in the addition of the fluctuative term $F_r^f = F_r^f\{(c_i^s)_{\mathrm{MFA}}\}$ to F_r in equation (I.45), as well as in the addition of the similar fluctuative corrections $F^f(c)$ to $F(c)$ and $\mu^f(c)$ to $\mu(c)$ in equation (4). The PCf approximation corresponds to employing for $F_r\{c_i\}$ in equation (4) the expression (I.45) with $c_i = (c_i^s)_{\mathrm{PCA}}$ and F_r^f given by equations (I.36) and (I.37) with $F_{ij}(g) = F_{ij}^{\mathrm{PCA}}(g)$, using for $F(c)$ equation (I.9) with $c_i = c$ and $K_{ij} = K_{ij}^{\mathrm{PCA}}$ determined by equation (I.13), while $\mu(c)$ is found as $N_s^{-1}\,\partial F(c)/\partial c$.

To find the fluctuative term F_r^f, equation (I.36), in the MFf or PCf approximation, we

Table 1. Characteristics of the nucleation for the fcc-1 alloy model at $T' = 0.5$. Here s is the reduced supersaturation given by equation (2); c is the initial alloy concentration; N_c and R_c^2 given by equation (10) are the total atom excess and the mean squared radius of the critical embryo, respectively; r_{nn} is the nearest-neighbour distance in the lattice; $\beta = 1/T$ is the reciprocal temperature; $\Delta\Omega_0$ and $\Delta\Omega_1$ are the values of the nucleation barrier (4) found in zeroth and first order in the fluctuations, respectively, as explained in section 4, while $\Delta\Omega_c$ is $\Delta\Omega_0 + \Delta\Omega_1$; γ_0 is the lowest, negative eigenvalue in the expansion (I.22) of the thermodynamic potential $\Omega\{c_i\}$ near its saddle point $c_i = c_i^s$; D_{aa} given by equation (I.55) is the generalized diffusivity along the critical direction in the c_i-space corresponding to growth of the embryo; $\mathcal{N}$ given by equation (I.43) is the normalizing constant in the embryo distribution function (I.42); $D_{\boldsymbol{R}}(\boldsymbol{u})$ given by equation (I.24) is the Jacobian of the 'translational' variables u_1, u_2, u_3 in equation (I.22) over the embryo centre coordinates R_1, R_2, R_3; v_a is the average volume per alloy atom; τ_e defined in the text after equation (9) is the characteristic time of the A $\leftrightarrow$ B atomic exchange in the alloy; and J_0 is the total prefactor (3).

Method	MFA or MFf					PCA or PCf				
s	0.10	0.20	0.30	0.45	0.60	0.10	0.20	0.30	0.45	0.60
c	0.034	0.046	0.059	0.078	0.096	0.025	0.035	0.045	0.060	0.076
N_c	212	56	29	19	16	238	64	36	25	22
R_c/r_{nn}	2.7	1.9	1.8	1.8	2.1	2.9	2.1	1.9	2.1	2.4
$\beta\,\Delta\Omega_0$	38.3	12.3	6.2	2.8	1.3	43.8	14.5	7.4	3.3	1.4
$\beta\,\Delta\Omega_1$	5.1	3.5	3.4	3.6	3.8	−1.7	2.9	4.0	4.7	4.8
$\beta\,\Delta\Omega_c$	43.5	15.8	9.7	6.4	5.0	42.1	17.4	11.5	7.9	6.2
$\beta\gamma_0$	−0.23	−0.47	−1.05	−1.60	−1.75	−0.22	−0.61	−1.11	−1.54	−1.58
$\tau_e D_{aa}$	0.40	0.38	0.41	0.37	0.40	0.29	0.29	0.28	0.27	0.25
$\mathcal{N}$	0.74	0.75	0.65	0.66	0.70	0.81	0.77	0.73	0.74	0.88
$v_a D_{\boldsymbol{R}}(\boldsymbol{u})$	41.4	7.7	2.3	0.7	0.2	49.7	9.0	3.1	0.9	0.3
$\tau_e v_a J_0$	2.36	0.60	0.26	0.08	0.03	2.15	0.62	0.26	0.09	0.03

need the fluctuation spectrum γ_m. Therefore, we should diagonalize the matrices $F_{ij}(g)$ in (I.34) which are of a high rank $r \sim 10^4$; see figure 5, later. To simplify the computations, we used the cubic symmetry of the crystal lattices under consideration. First we note that both the concentration distribution $c_i = c(\boldsymbol{r}_i - \boldsymbol{R})$ and the thermodynamic characteristics of the large critical embryo under consideration are virtually independent of the position of its centre $\boldsymbol{R}$. This is manifested, in particular, in the barrierless character of the translational diffusion of the embryo mentioned in section 3 of I, and it was also seen in a number of our calculations for various positions $\boldsymbol{R}$ in the crystal cell. Thus, to simplify the calculations, we took $\boldsymbol{R}$ to be positioned at the centre of the cubic crystal cell, which for the FCC lattice corresponds to an interstitial site, and for the BCC lattice corresponds to a lattice site. Then for both the FCC and BCC lattices the concentration distribution $c_i^s = c^s(\boldsymbol{r}_i - \boldsymbol{R})$ in the critical embryo has the full cubic symmetry. Therefore, the eigenvectors of the matrix $F_{ij}(g)$ at any g form one of the irreducible representations of the cubic group O_h. Using tables of these representations and their characters [6], we transform the matrix $F_{ij}(g)$ into the quasi-diagonal form corresponding to the irreducible representations. This reduces the rank of the matrix by about two orders of magnitude, and makes the diagonalization problem feasible.

For the cubically symmetric embryos under consideration, the Jacobian $D_{\boldsymbol{R}}(\boldsymbol{u})$, equation (I.24), has the form

$$D_{\boldsymbol{R}}(\boldsymbol{u}) = U_{11}^3 + U_{12}^3 + U_{13}^3 - 3U_{11}U_{12}U_{13} \tag{6}$$

Table 2. As table 1, but at $T' = 0.7$.

Method	MFA or MFf					PCA or PCf				
s	0.10	0.15	0.20	0.30	0.45	0.10	0.15	0.20	0.30	0.45
c	0.100	0.107	0.114	0.128	0.149	0.083	0.090	0.096	0.109	0.129
N_c	1320	472	237	101	51	1531	560	289	128	69
R_c/r_{nn}	5.2	3.8	3.2	2.7	2.5	5.4	4.0	3.4	2.9	2.8
$\beta\,\Delta\Omega_0$	54.5	25.9	15.3	7.1	3.0	66.6	32.0	19.0	9.0	3.8
$\beta\,\Delta\Omega_1$	99.2	32.8	16.5	8.2	5.8	7.4	3.4	3.6	4.4	5.1
$\beta\,\Delta\Omega_c$	153.7	58.7	31.8	15.3	8.8	73.9	35.4	22.6	13.4	8.9
$\beta\gamma_0$	−0.05	−0.08	−0.14	−0.28	−0.54	−0.05	−0.09	−0.15	−0.29	−0.54
$\tau_e D_{aa}$	0.31	0.30	0.28	0.27	0.25	0.23	0.22	0.21	0.20	0.18
$\mathcal{N}$	0.58	0.58	0.58	0.56	0.53	0.61	0.61	0.60	0.59	0.56
$v_a D_{\boldsymbol{R}}(\boldsymbol{u})$	199.7	64.7	28.7	8.7	2.3	237.6	78.3	35.5	11.1	3.0
$\tau_e v_a J_0$	3.03	1.29	0.70	0.28	0.09	2.80	1.29	0.71	0.28	0.09

Table 3. Characteristics of the nucleation for the bcc-1 alloy model at $T' = 0.7$.

Method	MFA or MFf				PCA or PCf			
s	0.10	0.15	0.30	0.45	0.10	0.15	0.30	0.45
c	0.100	0.107	0.128	0.149	0.075	0.081	0.100	0.119
N_c	1211	430	92	46	1542	571	135	73
R_c/r_{nn}	5.2	3.8	2.7	2.5	5.5	4.2	3.0	2.8
$\beta\,\Delta\Omega_0$	50.0	23.8	6.5	2.8	68.7	33.2	9.5	4.1
$\beta\,\Delta\Omega_1$	125.6	40.7	9.6	6.4	−7.4	−0.9	4.4	6.0
$\beta\,\Delta\Omega_c$	175.6	64.5	16.1	9.1	61.2	32.3	13.9	10.1
$\beta\gamma_0$	−0.04	−0.09	−0.28	−0.54	−0.05	−0.09	−0.29	−0.52
$\tau_e D_{aa}$	0.20	0.20	0.18	0.17	0.12	0.11	0.10	0.10
$\mathcal{N}$	0.59	0.58	0.56	0.53	0.63	0.63	0.60	0.57
$v_a D_{\boldsymbol{R}}(\boldsymbol{u})$	230.7	74.2	10.4	2.8	289.4	96.8	14.4	4.0
$\tau_e v_a J_0$	2.09	1.03	0.23	0.07	1.87	0.84	0.19	0.06

where $U_{11} = \partial u_1/\partial R_1 = \partial u_2/\partial R_2 = \partial u_3/\partial R_3$, $U_{12} = \partial u_1/\partial R_2 = \partial u_2/\partial R_3 = \partial u_3/\partial R_1$, and $U_{13} = \partial u_1/\partial R_3 = \partial u_2/\partial R_1 = \partial u_3/\partial R_2$. The derivatives $\partial u_\alpha/\partial R_\beta$ were found by numerical differentiation of the second of the equations (I.20) with the differentiation step equal to the lattice constant a. For example, the derivative U_{11} was found as

$$U_{11} = \frac{1}{a}\sum_{x_1,x_2,x_3} A_1(x_1,x_2,x_3)[c(x_1+a,x_2,x_3) - c(x_1,x_2,x_3)] \tag{7}$$

where $A_1(x_1, x_2, x_3)$ is $A_{i1} = A_1(\boldsymbol{r}_i - \boldsymbol{R})$ in equation (I.20) with $k = 1$, and x_1, x_2, and x_3 are the Cartesian components of the vector $\boldsymbol{r}_i - \boldsymbol{R}$. Our checks (as well as figures 2 and 3) show that such numerical differentiation provides sufficient computation accuracy. The results of these calculations are presented in tables 1–7 as the dimensionless quantities $v_a D_{\boldsymbol{R}}(\boldsymbol{u})$ where v_a is the average volume per atom—that is, $a^3/4$ for the FCC lattice, and $a^3/2$ for the BCC lattice.

To find the mobilities M_{ij} that enter equation (I.55) for the diffusivity D_{aa}, we use the

Table 4. Characteristics of the nucleation for the fcc-3 alloy model at $T' = 0.5$.

Method	MFA or MFf						PCA or PCf					
s	0.10	0.15	0.20	0.30	0.45	0.60	0.10	0.15	0.20	0.30	0.45	0.60
c	0.034	0.040	0.046	0.059	0.078	0.096	0.031	0.037	0.043	0.055	0.072	0.090
N_c	615	258	150	79	51	43	626	266	156	84	56	46
R_c/r_{nn}	3.9	3.1	2.7	2.5	2.5	2.9	3.9	3.1	2.7	2.5	2.6	2.9
$\beta\,\Delta\Omega_0$	104.8	53.8	33.6	16.9	7.5	3.4	108.7	56.1	35.2	17.8	7.9	3.5
$\beta\,\Delta\Omega_1$	3.9	3.0	3.1	3.3	3.5	3.8	−3.0	0.7	2.1	3.2	3.8	4.2
$\beta\,\Delta\Omega_c$	108.7	56.8	36.7	20.2	11.1	7.2	105.7	56.8	37.3	21.0	11.8	7.8
$\beta\gamma_0$	−0.19	−0.35	−0.54	−0.98	−1.56	−1.72	−0.19	−0.36	−0.56	−1.01	−1.56	−1.67
$\tau_e D_{aa}$	0.31	0.28	0.27	0.25	0.22	0.22	0.28	0.25	0.24	0.22	0.20	0.19
$\mathcal{N}$	0.73	0.73	0.71	0.68	0.65	0.69	0.74	0.74	0.73	0.69	0.67	0.73
$v_a D_{\boldsymbol{R}}(\boldsymbol{u})$	123.5	45.7	22.6	8.0	2.4	0.8	126.2	47.0	23.4	8.4	2.5	0.8
$\tau_e v_a J_0$	4.87	2.20	1.28	0.53	0.17	0.06	4.58	2.10	1.23	0.50	0.16	0.06

Table 5. As table 4, but at $T' = 0.6$.

Method	MFA or MFf				PCA or PCf			
s	0.10	0.20	0.30	0.45	0.10	0.20	0.30	0.45
c	0.060	0.074	0.088	0.108	0.056	0.069	0.083	0.102
N_c	1580	320	148	84	1622	334	158	91
R_c/r_{nn}	5.4	3.5	3.0	3.0	5.4	3.5	3.1	3.1
$\beta\,\Delta\Omega_0$	134.8	39.7	19.1	8.3	141.0	41.9	20.2	8.8
$\beta\,\Delta\Omega_1$	24.1	6.1	4.6	4.2	−4.9	1.6	3.1	3.9
$\beta\,\Delta\Omega_c$	158.9	45.8	23.7	12.5	136.1	43.5	23.3	12.7
$\beta\gamma_0$	−0.09	−0.27	−0.52	−0.94	−0.09	−0.28	−0.53	−0.94
$\tau_e D_{aa}$	0.25	0.23	0.20	0.18	0.22	0.20	0.18	0.16
$\mathcal{N}$	0.66	0.64	0.62	0.58	0.67	0.65	0.63	0.60
$v_a D_{\boldsymbol{R}}(\boldsymbol{u})$	267.6	42.7	14.1	4.0	275.0	44.4	14.8	4.2
$\tau_e v_a J_0$	5.03	1.29	0.51	0.16	4.77	1.24	0.49	0.16

results of the kinetic MFA and PCA approaches described in references [8, 9]. The MFA expression for M_{ij} has the form

$$M_{ij}^{\mathrm{MFA}} = \gamma_{ij}\left\{c_i c_i' c_j c_j' \exp\left[\beta \sum_k (u_{ik} + u_{jk}) c_k\right]\right\}^{1/2}. \tag{8}$$

Here γ_{is} is the configurationally independent factor in the probability of an atomic exchange A↔B between the sites i and s per unit time, and the 'asymmetric potential' u_{ij} is expressed via the inter-atomic interactions V_{ij}^{AA} and V_{ij}^{BB} between A or B atoms as $u_{ij} = V_{ij}^{\mathrm{AA}} - V_{ij}^{\mathrm{BB}}$.

The PCA results for the mobility can be obtained from the general expression for M_{ij} in the cluster-field approximation given in reference [9]. Neglecting for simplicity the inter-cluster correlations (which leads to an error of about ten per cent for the models

Table 6. As table 4, but at $T' = 0.7$.

Method	MFA or MFf						PCA or PCf					
s	0.10	0.15	0.20	0.30	0.45	0.60	0.10	0.15	0.20	0.30	0.45	0.60
c	0.100	0.107	0.114	0.128	0.149	0.170	0.095	0.101	0.108	0.122	0.143	0.164
N_c	3676	1310	663	281	142	104	3833	1375	700	300	155	114
R_c/r_{nn}	7.3	5.4	4.5	3.7	3.5	3.7	7.4	5.4	4.6	3.8	3.6	3.8
$\beta\,\Delta\Omega_0$	151.7	72.0	42.5	19.8	8.3	3.7	160.8	76.6	45.3	21.2	9.0	4.0
$\beta\,\Delta\Omega_1$	91.0	29.8	15.1	7.7	5.6	5.2	8.8	3.5	3.2	3.8	4.5	4.9
$\beta\,\Delta\Omega_c$	242.7	101.9	57.6	27.5	14.0	8.9	169.5	80.0	48.5	25.0	13.4	8.9
Ω_1/Ω_0	−0.030	−0.033	−0.036	−0.043	−0.056	−0.072	−0.030	−0.034	−0.037	−0.044	−0.057	−0.073
$\beta\gamma_0$	−0.04	−0.09	−0.14	−0.28	−0.54	−0.72	−0.04	−0.09	−0.14	−0.28	−0.54	−0.71
$\tau_e D_{aa}$	0.18	0.18	0.17	0.16	0.14	0.14	0.16	0.16	0.15	0.14	0.12	0.13
$\mathcal{N}$	0.58	0.58	0.57	0.56	0.53	0.52	0.59	0.59	0.58	0.57	0.54	0.53
$v_a D_{\boldsymbol{R}}(\boldsymbol{u})$	438.5	143.2	64.6	20.4	5.5	1.7	457.8	150.2	68.1	21.6	5.9	1.8
$\tau_e v_a J_0$	3.75	1.70	0.94	0.37	0.12	0.04	3.61	1.64	0.91	0.36	0.12	0.04

Table 7. As table 4, but at $T' = 0.8$.

Method	MFA or MFf				PCA or PCf			
s	0.20	0.30	0.45	0.60	0.20	0.30	0.45	0.60
c	0.171	0.184	0.204	0.224	0.165	0.178	0.198	0.218
N_c	1433	568	269	187	1537	614	294	206
R_c/r_{nn}	6.0	4.9	4.5	4.8	6.2	5.0	4.6	4.9
$\beta\,\Delta\Omega_0$	40.8	18.6	7.7	3.4	44.1	20.1	8.3	3.7
$\beta\,\Delta\Omega_1$	40.2	15.8	8.5	6.8	13.6	7.6	6.0	5.9
$\beta\,\Delta\Omega_c$	81.0	34.4	16.2	10.2	57.7	27.7	14.4	9.6
$\beta\gamma_0$	−0.07	−0.14	−0.28	−0.41	−0.07	−0.14	−0.28	−0.40
$\tau_e D_{aa}$	0.11	0.10	0.09	0.09	0.10	0.10	0.08	0.09
$\mathcal{N}$	0.51	0.50	0.49	0.48	0.52	0.51	0.49	0.48
$v_a D_{\boldsymbol{R}}(\boldsymbol{u})$	79.0	24.1	6.4	1.9	84.8	26.1	6.9	2.1
$\tau_e v_a J_0$	0.48	0.19	0.06	0.02	0.47	0.19	0.06	0.02

used), we obtain

$$M_{ij}^{\mathrm{PCA}} = \gamma_{ij} c_i' c_j' \exp\left[\frac{\beta}{2}\left(\frac{\partial F}{\partial c_i} + \frac{\partial F}{\partial c_j}\right) + \sum_{k\neq i,j} \ln(1 + f_k^{ij} c_k)\right] \tag{9}$$

where $F = F_{\mathrm{PCA}}$ is given by equation (I.12), and f_k^{ij} is $\exp[\beta(u_{ik} - v_{ik} + u_{jk} - v_{jk})/2] - 1$. In the case of the applicability of the MFA, $|\beta u_{ij}|, |\beta v_{ij}| \ll 1$, equation (9) turns into (8). The PCA expression for the mobility will be discussed in more detail elsewhere.

For numerical estimates, we use the nearest-neighbour exchange model, i.e. we set the atomic jump probability γ_{is} in equations (8) and (9) to be $1/\tau_e$ when the sites i and s are nearest neighbours, and zero otherwise; the quantity τ_e is evidently the characteristic time for position exchange of neighbouring A and B atoms in an alloy. The asymmetric potentials u_{ij} in equations (8) and (9) are taken to be zero.

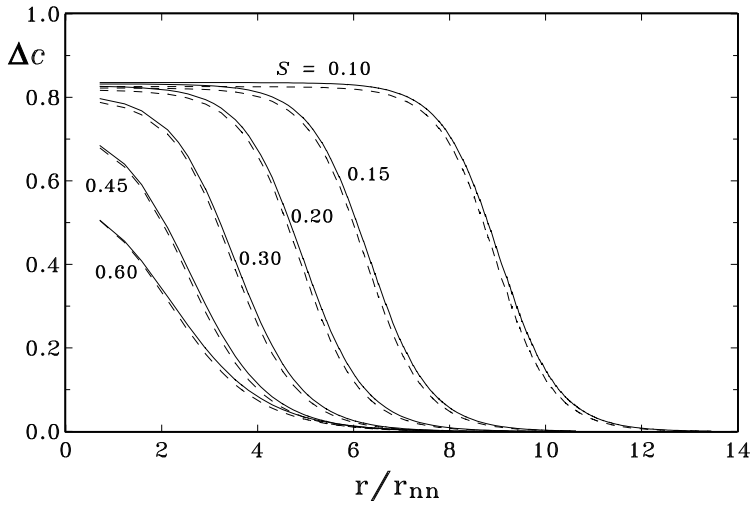

Figure 2. Concentration profiles $\Delta c(r) = c(r) - c$ of the critical embryo for the model fcc-3 at $T' = 0.7$ at various supersaturations s defined by equation (2). For clarity, the values of $\Delta c(r)$ at neighbouring discrete points $r = r_i$ are connected with lines. Solid curves: the PCA; dashed curves: the MFA.

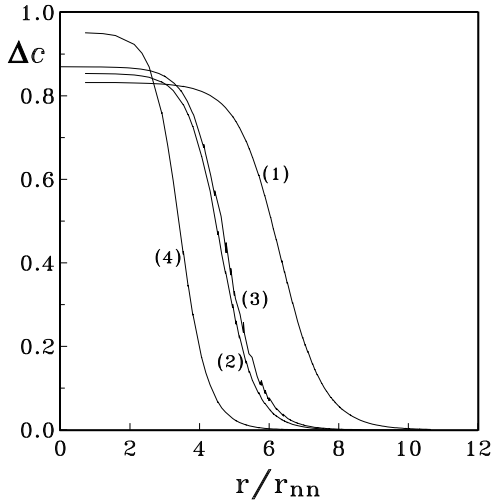

Figure 3. As figure 2, found in the PCA at the supersaturation $s = 0.15$ for the following models and temperatures: curve 1: fcc-3 at $T' = 0.7$; curve 2: fcc-1 at $T' = 0.7$; curve 3: bcc-1 at $T' = 0.7$; curve 4: fcc-3 at $T' = 0.5$.

4. Results of the calculations

The results of our calculations are presented in tables 1–7 and figures 1–6. The reduced temperature T' in the tables and figures is the ratio T/T_c, where T_c is the critical temperature found for the model under consideration in the approximation used. The 'Method' row in the tables indicates which of the above-discussed approximations for $F\{c_i\}$ (the MFA, MFf, PCA or PCf) is employed in the calculation. The quantity s is the reduced supersaturation

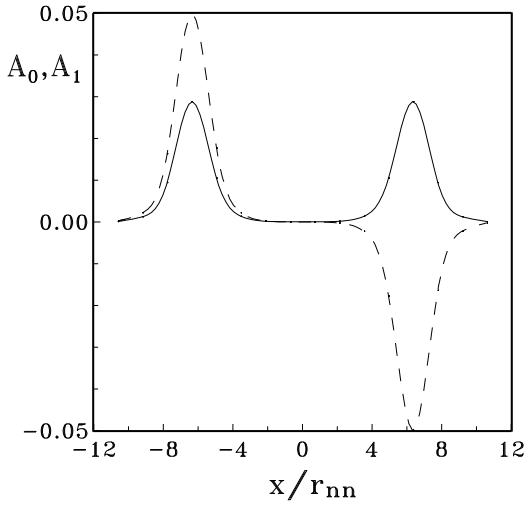

Figure 4. Profiles of the coefficients $A_{i0} = A_0(\boldsymbol{r}_i)$ and $A_{i1} = A_1(\boldsymbol{r}_i)$ in equation (I.20) across the diameter of the critical embryo, $\boldsymbol{r}_i = (x, 0, 0)$, found in the PCA for the model fcc-3 at $T' = 0.7$ and $s = 0.15$. Solid curve: $A_0(x)$; dashed curve: $A_1(x)$.

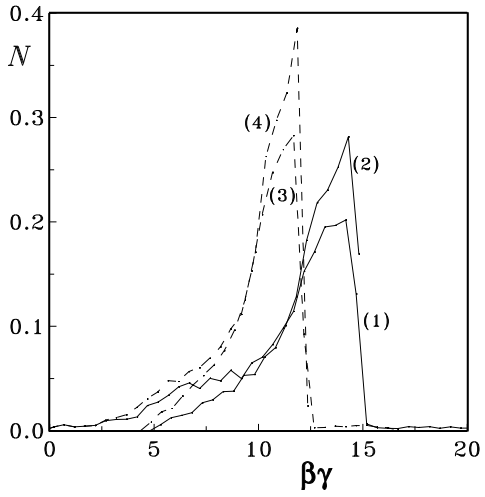

Figure 5. The density of states $N(\beta\gamma)$ for the concentration fluctuation spectrum found as described in the text for the fcc-1 model at $s = 0.15$ and $T' = 0.7$. Solid lines: the PCA; dashed lines: the MFA. Curves 1 and 3 correspond to the state with the critical embryo; curves 2 and 4 correspond to the initial uniform metastable state.

(2) for the initial metastable state, while c is the concentration that corresponds to that s. N_c is the total excess of the A-species atoms in the critical embryo with respect to the initial state, and R_c^2 is the mean squared radius of the embryo:

$$N_c = \sum_i (c_i - c) \qquad R_c^2 = \frac{1}{N_c} \sum_i r_i^2 (c_i - c) \tag{10}$$

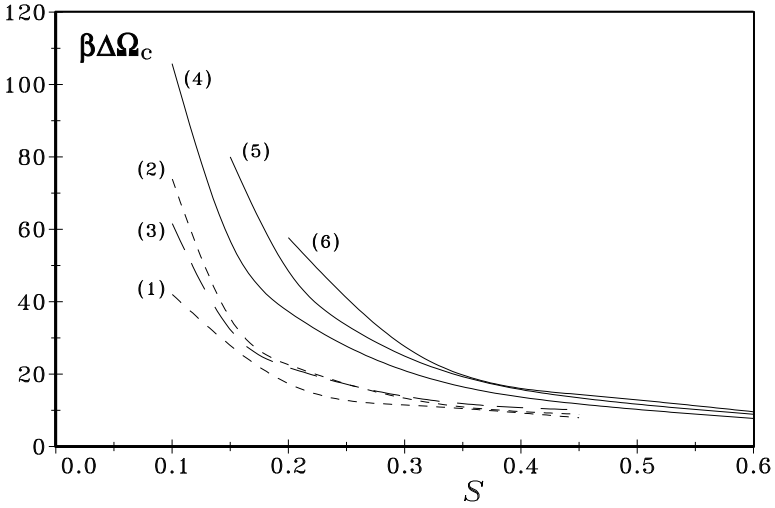

Figure 6. Values of the reduced nucleation barrier $\beta\,\Delta\Omega_c$ given by equation (4) versus the reduced supersaturation s found in the PCf approximation. Key to curves: dashed lines: fcc-1 model: (1) $T' = 0.5$, (2) $T' = 0.7$; long-dashed line: bcc-1 model: (3) $T' = 0.7$; solid lines: fcc-3 model: (4) $T' = 0.5$, (5) $T' = 0.7$, (6) $T' = 0.8$.

while r_{nn} is the nearest-neighbour distance, equal to $a/\sqrt{2}$ in the FCC lattice, and to $a\sqrt{3}/2$ in the BCC lattice. The values $c_i = c_i^s$ in equation (10) correspond to the critical embryo, while r_i is the distance from the site i to the embryo centre $\boldsymbol{R}$.

The quantities $\Delta\Omega_0$ and $\Delta\Omega_1$ in tables 1–7 are the terms in the sum $\Delta\Omega_c = \Delta\Omega_0 + \Delta\Omega_1$ which are of zeroth and first order in the fluctuative contribution, respectively. For the MFA and MFf approximations, $\Delta\Omega_0$ is $\Delta\Omega_{\rm MFA}$ which corresponds to using the MFA expression (I.46) for both F_r and $F(c)$ in equation (4): $F_r\{c_i\} = F_{\rm MFA}\{c_i\}$ with $c_i = (c_i^s)_{\rm MFA}$; $F(c) = F_{\rm MFA}\{c_i\}$ with $c_i = c$; and $\mu(c) = N_s^{-1}\,\partial F(c)/\partial c$. Similarly, for the PCA and PCf approximations, $\Delta\Omega_0$ is $\Delta\Omega_{\rm PCA}$, which corresponds to using the PCA expressions (I.12) for both $F_r\{c_i\}$ and $F(c)$ in equation (4), with $c_i = (c_i^s)_{\rm PCA}$ and $c_i = c$, respectively. The quantity $\Delta\Omega_1$ for both the MFf and PCf approximations can be written as

$$\Delta\Omega_1 = F_r^f\{c_i\} - F^f(c) - \mu^f(c)\sum_i (c_i - c). \tag{11}$$

For the MFf approximation, the values of c_i in equation (10) are $(c_i^s)_{\rm MFA}$, $F_r^f\{c_i\}$ is $F_r^f\{c_i\}$ given by equation (I.36) or (5), $F^f(c) = F_{\rm MFA}^f(c)$ is given by the last term of equation (I.9) at $c_i = c$ and $K_{ij} = K_{ij}^{\rm MFA}$, while $\mu^f(c)$ is $N_s^{-1}\,\partial F^f(c)/\partial c$. For the PCf approximation, the c_i-values in equation (11) are $(c_i^s)_{\rm PCA}$, while the fluctuative contribution $F_r^f\{c_i\}$, $F^f(c)$ or $\mu^f(c)$ is defined as the difference between the PCf and PCA results for each quantity. Therefore, $F_r^f\{c_i\}$ is the difference $F_r^{\rm PCf}\{c_i\} - F_{\rm PCA}\{c_i\}$ where $F_r^{\rm PCf}\{c_i\}$ is given by equation (I.45) with F_r^f defined by equations (I.36) and (I.37) for $F_{ij}(g) = F_{ij}^{\rm PCA}$. Similarly, $F^f(c)$ is the difference $F_{\rm PCf}(c) - F_{\rm PCA}(c)$ with $F_{\rm PCf}(c)$ given by equation (I.16) with $c_i = c$, while $\mu^f(c)$ is $N_s^{-1}\,\partial F^f(c)/\partial c$. The quantity Ω_1/Ω_0 in table 6 is the ratio $\Omega_1(c)/\Omega_0(c)$ for the initial metastable state, where

$$\Omega_0(c) = F_0(c) - \mu_0(c)N_0 \qquad \Omega_1(c) = F^f(c) - \mu^f(c)N_0. \tag{12}$$

Here N_0 is $N_s c$ where N_s is the total number of lattice sites, $F_0(c)$ and $\mu_0(c)$ in the MFf

approximation are $F_{\mathrm{MFA}}(c)$ and $\mu_{\mathrm{MFA}}(c)$, and in the PCA approximation they are $F_{\mathrm{PCA}}(c)$ and $\mu_{\mathrm{PCA}}(c)$, while $F^f(c)$ and $\mu^f(c)$ in equation (12) are the same as in equation (11).

5. Discussion of the results

Let us discuss the results of the calculations. First we note that they agree with the qualitative conclusions of Cahn and Hilliard [3] concerning the variation of the parameters of the critical embryo with increasing supersaturation s: the nucleation barrier $\Delta\Omega_c$ lowers, the interface with the exterior phase gets more diffuse, and the composition within the embryo approaches that of the exterior phase. The calculated embryo radius R_c with increasing s at first decreases, but then begins to increase, which also agrees with the results of [3]; in our calculations the minimum of $R_c(s)$ is positioned at $s \gtrsim 0.45$. However, as is discussed below, at such high s the approach employed in this and previous work [2–4], which treats an isolated embryo neglecting its interaction with other ones, loses its validity. Therefore, the results of the calculations for such high values of s may have no physical meaning.

At a given supersaturation s, the values of R_c and N_c sharply rise with increasing temperature T. To qualitatively interpret this, one can employ the classical model in which the embryo is treated as a homogeneous droplet with sharp boundaries [4]. The critical radius R_c in this model is proportional to the ratio of the surface tension coefficient α to the grand canonical potential per site difference $\delta\omega = [\Omega(c, T) - \Omega(c_b, T)]/N_s$; the factors α and $\delta\omega$ determine the thermodynamic loss and thermodynamic gain, respectively, in the formation of the embryo [4]. Thus the above-mentioned rise of R_c can imply that with increasing T at fixed s the difference $\delta\omega(T)$ decreases more rapidly than the surface tension $\alpha(T)$. For actual embryos with diffuse boundaries, similar qualitative conclusions may be applied to some averaged characteristics of the surface thermodynamic loss $\langle\alpha\rangle$ and the volume thermodynamic gain $\langle\delta\omega\rangle$.

Comparisons of the R_c-values for the fcc-1 and fcc-3 models given in tables 1 and 5, 3 and 6, and in figure 3 illustrate a notable dependence of the embryo size R_c on the interaction radius r_{int}; in our results, R_c is approximately proportional to r_{int}. This can imply a similar dependence on r_{int} of the above-mentioned 'effective surface tension' $\langle\alpha\rangle$, which correlates with the linear dependence on r_{int} of the usual inter-phase surface tension in the Ginzburg–Landau theory [7].

The values of N_c in tables 1–7 show that the critical embryo includes a great number of atoms for all of the alloy systems considered. Therefore, the number of sites N_e within the embryo is always large: $N_e > N_c \gg 1$, which was repeatedly mentioned and made use of in I.

Figures 2 and 3 show the concentration profile of the critical embryo, $\Delta c(r) = c(r) - c$. When at a given $r = |\boldsymbol{r}_i|$ there are several non-equivalent vectors $\boldsymbol{r} = \boldsymbol{r}_i$, such as the vectors $(3, 3, 3)a/2$ and $(5, 1, 1)a/2$ in the BCC lattice, then several values $\Delta c(\boldsymbol{r}_i)$ for that $|\boldsymbol{r}_i| = r$ are presented in the figures; this causes vertical peaks in the curves $\Delta c(r)$. The profiles show that the concentration distribution in the embryo is approximately spherical, particularly when the configurational interaction spreads beyond the nearest neighbour, which is the case for the fcc-3 model. However, for the nearest-neighbour interaction models, particularly for the bcc-1 model, irregularities in $\Delta c(r)$ reflecting a non-sphericity in the concentration distribution are distinctly seen in figure 3. The difference in $\Delta c(r)$ between the fcc-1 and bcc-1 models in figure 3 is small; thus the lattice structure has little effect on the concentration profile.

Figure 4 illustrates the physical meaning of the concentrational modes u_0 and u_1 in equations (I.20)–(I.22). According to the second of equations (I.20), the quantity

$A_{i0} = A_0(\boldsymbol{r}_i)$ or $A_{i1} = A_1(\boldsymbol{r}_i)$ determines the change of the concentration distribution $c_i = c(\boldsymbol{r}_i)$ under the variation of the variable u_0 or u_1. Comparison of figures 4 and 3 shows that the variation δu_0 corresponds to the variation of the size of the embryo, i.e. the shifting of its boundary outwards at $\delta u_0 > 0$ or inwards at $\delta u_0 < 0$, while δu_1 corresponds to the shift of the embryo as a whole along the x-axis.

The reduced eigenvalue $\beta\gamma_0$ in tables 1–7 characterizes the negative curvature of the thermodynamic barrier $\Delta\Omega\{c_i\}$ (I.19) at its saddle point. The value $|\beta\gamma_0|$ decreases with increasing temperature and increases with increasing supersaturation, being zero at the binodal when $s = 0$ and becoming of the order of unity at $s \gtrsim 0.6$. With further increasing s, the value of $|\beta\gamma_0|$ begins to decrease, and it vanishes again at the spinodal when $s = 1$, but, as mentioned above, calculations for such high values of s may have little physical meaning. The geometric factor $D_{\boldsymbol{R}}(\boldsymbol{u})$ in tables 1–7 varies with s and T similarly to the total volume or the total atom excess N_c in the embryo, sharply increasing with decreasing s or increasing T. Unlike $\beta\gamma_0$ and $D_{\boldsymbol{R}}(\boldsymbol{u})$, the diffusivity D_{aa} and the normalizing factor $\mathcal{N}$ in tables 1–7 both exhibit a weak dependence on s and T. Therefore, the s- and T-dependence of the prefactor J_0 in equations (1) and (3) is mainly determined by that of the factor $D_{\boldsymbol{R}}(\boldsymbol{u})$; in particular, J_0 notably decreases with increasing supersaturation s.

Let us now discuss the results for the nucleation barrier $\Delta\Omega_c$. First we discuss the importance of the fluctuative effects for this quantity. The zero-order values $\Delta\Omega_0$ in tables 1–7 correspond to the MFA or PCA results for $\Delta\Omega_c$. As discussed in I, in the MFA the fluctuative effects are neglected, while the PCA takes into account only the pair correlations of fluctuations and neglects the many-site ones. Comparing the values of $\Delta\Omega_0$ in tables 1–7, we see that for the nearest-neighbour interaction models the values of $\Delta\Omega_{\mathrm{PCA}}$ notably exceed those of $\Delta\Omega_{\mathrm{MFA}}$, by 20–30% for the fcc-1 model, and by 40–50% for the bcc-1 model. Therefore, the errors in the simple MFA approach in evaluations of the nucleation barrier for systems with short-range interactions can be significant. For the fcc-3 model the values of $\Delta\Omega_{\mathrm{MFA}}$ and $\Delta\Omega_{\mathrm{PCA}}$ are close to each other, in accordance with the well-known decreasing of fluctuative effects with increasing interaction range [10].

The MFf approximation treats the fluctuative contribution as a first-order perturbative correction to the zero-order MFA result, which is appropriate only when the correction is not large. In our problem, this means that the ratio $r_{\mathrm{MF}} = \Delta\Omega_1^{\mathrm{MFf}}/\Delta\Omega_{\mathrm{MFA}}$ should be small. Similarly, the PCf approximation corresponds to the perturbative treatment of the non-pair correlations disregarded in the PCA [1], and thus it is applicable when the ratio $r_{\mathrm{PC}} = \Delta\Omega_1^{\mathrm{PCf}}/\Delta\Omega_{\mathrm{PCA}}$ is small. It is also known that for uniform systems the MFf approximation usually overestimates the fluctuative contributions, particularly in the phase transition region [10].

The results for $\Delta\Omega_1$ and $\Delta\Omega_0$ given in tables 1–7 show that the relative importance of the fluctuative effects, as characterized by the value of r_{MF} or r_{PC}, sharply rises with both T and s. The rise with temperature is natural, by general considerations, while the rise with supersaturation seems to be mainly related to the increase of the embryo boundary smearing illustrated in figure 2. The structure of the atomic distribution near the boundary appears to be much more soft and flexible than that in the homogeneous system. This results in an enhancement of the concentration fluctuations in this region, and thus their thermodynamic contribution rises.

This softening of the fluctuation spectrum is illustrated in figure 5, which presents the density of states $N(\beta\gamma)$ for the quantities $\beta\gamma = \beta\gamma_k$ where γ_k entering equation (I.22) is the eigenvalue of the matrix $F_{ij} = \partial^2 F/\partial c_i\,\partial c_j$. The values of $N(\beta\gamma)$ in figure 5 were found by sampling of the $\beta\gamma_k$-values over the intervals $\Delta(\beta\gamma_k) = 0.5$, while the total number of γ_k used in this calculation (equal to the number of sites in the simulation region) was

7136. According to equations (I.8) and (I.22), the quantity $1/\beta\gamma_k$ is the mean squared fluctuation amplitude for the fluctuative eigenmode u_k; thus the fluctuative thermodynamic contribution increases with decreasing $\beta\gamma_k$. In particular, in the MFf approximation the increase is described by equation (5). Figure 5 shows that the softening of the fluctuation spectrum is very pronounced, and in the PCf approximation it is still stronger than in the less accurate MFf one. The 'soft' fluctuations correspond mainly to surface modes—in particular, to variations of the shape of the embryo. Figure 5 also shows the presence of some 'stiff' concentrational modes with large values of $\beta\gamma_k$ that correspond to the fluctuations localized well within the embryo. However, the total number of such stiff modes and their thermodynamic contribution are small.

Let us now discuss the values of the above-mentioned ratio r_{MF} or r_{PC} that characterize the applicability of the MFf or PCf approximation. Finding these ratios with the use of tables 1–7, we see that for the MFf approximation the applicability region is rather narrow. For the nearest-neighbour interaction systems considered, the r_{MF}-value is small only for the fcc-1 model at the lowest $T' = 0.5$ and $s = 0.1$. Even for the fcc-3 model (for which the interaction range is large and the fluctuative effects are suppressed [10]), the ratio r_{MF} is small only at low $T' = 0.5$–0.6 and low $s \lesssim 0.3$. At the same time, the analogous parameter r_{PC} for the PCf approximation remains small over broad intervals of T' and s even for the nearest-neighbour interaction models. However, with increasing supersaturation s the r_{PC}-value becomes no longer small, too; for the nearest-neighbour interaction models, this happens at $s \gtrsim 0.3$, and for the fcc-3 model, at $s \gtrsim 0.45$.

The increase of the fluctuative effects is entirely due to the above-mentioned softening of the fluctuation spectrum in such non-uniform systems as embryos. This is illustrated by the values of $r(c) = \Omega_1/\Omega_0$ in table 6 which are analogues of r_{MF} or r_{PC} but for the uniform metastable state. We see that the values of $r(c)$ remain small at all supersaturations s for both the MFf and the PCf approximation.

Therefore, for the non-uniform systems under consideration, the MFf approximation appears to overestimate the fluctuative effects even more strongly than it does in the homogeneous case. At the same time, the PCf approach in our problem seems to have a sufficiently wide applicability region, and at moderate $s \lesssim 0.3$–0.45 this approach seems to be the most accurate of the ones used in this work. Therefore, the final estimates of the nucleation barrier $\Delta\Omega_c$ presented in figure 6 employ the PCf approximation. However, with further increasing supersaturation the fluctuative effects become really large, and all of the calculations of this work become unreliable.

Let us now discuss the limitations of the theory related to its main physical assumptions rather than to methodological difficulties. The approach employed [1–4] considers the isolated embryo within an otherwise unperturbed metastable state, and neglects interactions of different embryos. This assumes a negligible probability of finding another embryo within the characteristic volume $v_c \sim l_c^3$ during the time interval t_c which is important for the process. Therefore, the nucleation rate J in equation (1) should obey the inequality

$$J t_c l_c^3 \ll 1. \tag{13}$$

The lower limit for the time $t_c = t_c(l_c)$ can be estimated from the condition that it should be sufficient for the processes of the approximate equilibration of the concentration distribution around the critical embryo to take place. Therefore, t_c should exceed the characteristic time needed for diffusion over the distance l_c: $t_c > l_c^2/D$ where $D \simeq r_{nn}^2/\tau_e$ is the atomic diffusivity. On the other hand, in order for the different embryos not to affect each other, the characteristic size l_c should significantly exceed the embryo diameter $2R_c$. If we take for l_c, say, $l_c \sim 4R_c$, and take the estimate $r_{nn}^3 \sim v_a$, where v_a is the average volume per

atom, inequality (13) takes the form

$$10^3(\tau_e v_a J_0)\exp(-\beta\,\Delta\Omega_c)(R_c/r_{nn})^5 \ll 1. \tag{14}$$

The numerical factor in the lhs of this inequality is most probably underestimated. For example, we did not take into account the restrictions on the time t_c related to the conservation of the total number of atoms, which would result in $(1/c)$-type factors in the lhs of equation (14). However, such refinements would hardly significantly affect the numerical estimates given below.

Using for the parameters J_0, $\Delta\Omega_c$, and R_c in inequality (14) their values given in tables 1–7 for the PCf approximation, we find that for the nearest-neighbour interaction models the inequality corresponds to $s \lesssim 0.3$–0.35, and for the fcc-3 model it corresponds to $s \lesssim 0.45$, while the temperature dependence of the lhs of equation (14) is relatively weak. Therefore, the reduced supersaturation s appears to be the main factor determining the nucleation rate, for the models considered anyway. Let us also note that these limiting values of s are numerically close to those determined from the above-discussed condition of the relative insignificance of fluctuative effects in the thermodynamics of nucleation.

Even when inequality (14) is obeyed, the approach used [1–4] requires the total time t of the process to be not too long in order for the total amount of the new phase to be relatively small. The relevant restrictions on t can be found from atom-number-conservation considerations.

6. Conclusions

Let us summarize the main results of this work. To get an idea of the characteristics of homogeneous nucleation in alloys, we used the microscopical theory developed in the preceding paper [1] to calculate the nucleation rate and the parameters of the critical embryo for several alloy models. The nearest-neighbour interaction models for the FCC and BCC lattices (the fcc-1 and bcc-1 models) and the third-neighbour interaction model for the FCC lattice (the fcc-3 model) have been considered. The results of the calculations show that the nucleation rate is mainly determined by three ruling parameters: the reduced supersaturation s defined by equation (2), the reduced temperature $T' = T/T_c$ where T_c is the critical temperature, and the ratio of the interaction radius r_{int} defined in section 2 to the nearest-neighbour distance r_{nn}. These parameters can also be useful for analysing the nucleation in other systems, such as vapours or liquids. With increasing supersaturation s, the nucleation barrier $\Delta\Omega_c$ lowers, the interface of the critical embryo with the exterior phase gets more diffuse, and the composition within the embryo approaches that of the exterior phase, in qualitative agreement with the conclusions of Cahn and Hilliard [3] reached with the use of a simplified treatment. At all of the values of s, T considered, the critical embryo is large, i.e. includes a great number of sites. The excess of atoms, N_c, and the radius R_c of the critical embryo increase sharply with decreasing supersaturation s and increasing temperature T. With increasing interaction radius r_{int}, the embryo radius R_c rises approximately linearly; this can be understood in terms of the classical sharp-boundary model of the critical embryo [4] if one accepts the Ginzburg–Landau approach result [7], namely that the dependence of the inter-phase surface tension on r_{int} is linear. The concentration distribution $c(\boldsymbol{r})$ of the critical embryo is approximately spherical, but a slight non-sphericity of $c(\boldsymbol{r})$ is clearly seen in the nearest-neighbour interaction systems, particularly for the bcc-1 model.

The prefactor J_0 in the Zeldovich–Volmer relation (1) notably decreases with increasing supersaturation, typically by two orders of magnitude between $s = 0.1$ and $s = 0.6$, while its temperature dependence at fixed s is relatively weak. The calculations of the

nucleation barrier $\Delta\Omega_c$ carried out using various approximations for the free energy of a non-uniform alloy, $F\{c_i\}$, show that the use of the mean-field approximation (MFA) for the nearest-neighbour interaction models can lead to significant underestimation of $\Delta\Omega_c$ with respect to the more accurate pair-cluster approximation (PCA): by 20–30% for the fcc-1 model, and by 40–50% for the bcc-1 model. For the fcc-3 model where the interaction range is larger, the MFA and PCA results for $\Delta\Omega_c$ are close to each other. The thermodynamic contribution of the composition fluctuations to $\Delta\Omega_c$ sharply rises with increasing supersaturation. This reflects a considerable softening of the fluctuation spectrum for highly inhomogeneous systems, and an increase of the fluctuation amplitudes in the region of the diffuse surface of the embryo which is related to the diffuse character of its boundary. However, employing the 'pair-cluster-with-fluctuations' approximation $F_{\mathrm{PCf}}\{c_i\}$ suggested in [1] enables one to quantitatively describe the fluctuative contributions over broad intervals of supersaturation, for $s \lesssim 0.3$ for the nearest-neighbour interaction models, and for $s \lesssim 0.45$ for the fcc-3 model. At higher s the fluctuative effects become large, and the calculation methods used in this work become unreliable.

The more important restriction on the applicability of the theoretical approach used [1–4] is related to the neglect of the interactions of different embryos. The estimates (13), (14) made with the use of our numerical results show that such effects limit the applicability region to supersaturation values that are not too high, namely $s \lesssim 0.3$–0.35 for the nearest-neighbour interaction models, and $s \lesssim 0.45$ for the fcc-3 model. These limits are numerically close to the above-mentioned conditions for the relative insignificance of fluctuative effects in the thermodynamics of nucleation. However, within these limits, the microscopical approach developed in this work seems to provide a way of treating the homogeneous nucleation in alloys consistently.

Acknowledgments

The authors are much indebted to Georges Martin for numerous stimulating discussions and for his interest during the work on this problem. The work was supported by the Russian Fund for Basic Research under Grant No 97-02-17842.

References

[1] Dobretsov V Yu and Vaks V G 1998 *J. Phys.: Condens. Matter* **10** 2261
[2] Zeldovich Ya B 1942 *Zh. Eksp. Teor. Fiz.* **12** 525
Lifshitz E M and Pitaevsky L P 1979 *Physical Kinetics* (Moscow: Nauka) §99
[3] Cahn J W and Hilliard J E 1959 *J. Chem. Phys.* **31** 688
[4] Landau L D and Lifshitz E M 1976 *Statistical Physics* (Moscow: Nauka) §162
[5] Turchi P E A 1994 *Principles (Intermetallic Compounds 1)* ed J H Westbrook and R L Fleischer (New York: Wiley) pp 21–54
[6] Kovalev O V 1986 *Irreducible and Induced Representations and Co-representations of Fedorov's Groups* (Moscow: Nauka)
[7] Landau L D and Lifshitz E M 1976 *Electrodynamics of Continuous Media* (Moscow: Nauka) §43
[8] Vaks V G, Beiden S V and Dobretsov V Yu 1995 *Pis. Zh. Eksp. Teor. Fiz.* **61** 65 (Engl. Transl. 1995 *JETP Lett.* **61** 68)
[9] Vaks V G 1996 *Pis. Zh. Eksp. Teor. Fiz.* **63** 447 (Engl. Transl. 1996 *JETP Lett.* **63** 471)
[10] Vaks V G, Larkin A I and Pikin S A 1966 *Zh. Eksp. Teor. Fiz.* **51** 361